Supporting Information for Publication

Solving the enigma of weak fluorine contacts in solid state: a periodic DFT study of fluorinated organic crystals

Elena O. Levina [a), f)], Ivan Y. Chernyshov [b)], Alexander P. Voronin [c)], Leonid N. Alekseiko [d)], Adam I. Stash [e)], M.V. Vener [*g)]

[a)] *Moscow Institute of Physics and Technology, Dolgoprudny, Russia*

[b)] *N.D. Zelinsky Institute of Organic Chemistry, Moscow, Russia*

[c)] *G.A. Krestov Institute of Solution Chemistry of RAS, Ivanovo, Russia*

[d)] *Far Eastern Federal University, Vladivostok, Russia*

[e)] *Karpov Institute of Physical Chemistry, Moscow, Russia*

[f)] *Research Centre of Biotechnology, Russian Academy of Sciences, Moscow, Russia*

[g)] *D. Mendeleev University of Chemical Technology, Moscow, Russia*

[*]*Corresponding author*: Mikhail V. Vener, e-mail: mikhail.vener@gmail.com

Table of contents

Details of plane-wave DFT computations

Quantum Expresso (version 6.2) [1, 2] was used for all pseudopotential plane-wave calculations. The Quantum Expresso calculations were carried out with the PBE and PBESOL functionals with Troullier-Martins [3] and Hartwigsen-Goedeker-Hutter [4] norm-conserving pseudopotentials, Rappe-Rabe-Kaxiras-Joannopoulos ultrasoft pseudopotentials [5, 6] and PAW pseudopotentials [7] for core electrones. Crystalline tetrafluoromethane (**CF_4**) and pentafluorobenzoic acid (**C_6F_5COOH**) were chosen for test calculations. The kinetic energy cutoff was set to 110 Ry, which is common for calculations of crystals containing first-row elements [8]. It was found that 36-poins in *k*-sapling are enough for test calculations, because increase in number of *k*-points did not affect on the results. However, decrease of *k*-points number sometimes led to problems with SCF convergence. Tolerance on energy controlling the self-consistent field convergence for geometry optimization was set to 1×10^{-8} Hartree. Two algorithms for geometry optimization were used: the damped dynamics and the BFGS quasi-newton algorithm. The cell parameters and the space group were fixed during the geometry optimisation process.

According to our computations, it is possible to carry out geometry optimization for **C_6F_5COOH**, which gives reasonable structure, but in case of **CF_4** we couldn't achieve reasonable geometry. After several steps of geometry optimization process (or even sometimes after first step) the molecules deformed and the bond lengths became too high for covalent C-F bounds (~2 Å). Due to above-stated difficulties with geometry optimization of **CF_4**, we conclude that applicability of the pseudopotential plane-wave calculations to some organic crystals with perfluorated molecules is not straightforward.

Three additional sets of molecular crystals

Three additional sets of molecular crystals are considered. The first set includes the crystals, for which experimental and theoretical values of the electron density and it's Laplacian at the (3,-1) critical point of the C-F···F-C interactions are available. Pentafluorobenzoic acid (**C_6F_5COOH**) [9], 2,3,5,6-tetrafluoropyridine (**C_5NHF_4**) [10], 3,4,5,6-Tetrafluoro-1,2-benzenedicarbonitrile (**GEYLOL01**) [11], 4-Fluorobenzamide (**BENAFP02**) [12], 4,4'-bis(perfluorophenyl)-2,2'-bithiazole (**KETVUC01**) [13]. Crystals with the C-F···F-C interactions and conventional H-bonds formed the second set. 4-deoxy-4-fluoro-1,3,5-o-methylidyne-myo-inositol (**TISQER**) [14], 12,12,13,13,14,15,15-octafluorohexacosanedioic acid (**R_fCOOH**) [15] and **C_6F_5COOH**. Crystals of 1-(4-Fluorobenzoyl)-3-(isomeric fluorophenyl)thioureas **OVIHAD, OVIHEH** and **OVIHIL** [16] formed the third set.

The theoretical background of gradient fields evaluation.

According to Bader's theory [17], the ρ-basins are regions divided by surface $S(r)$ of zero flux in the gradient vectors of electron density:

$$\nabla\rho(r)\cdot n(r)=0; r\in S(r) \tag{s1}$$

Here $n(r)$ is the unit vector directed normally towards surface $S(r)$ at point r. The ρ-basin of each nucleus defines bounded atoms (so-called pseudoatoms) in the crystal [17].

The inner electrostatic field in crystal is characterized by electrostatic potential:

$$v(r)=\sum_{A}\frac{Z_A}{|R_A-r|}-\int\frac{\rho(r')dr'}{|r-r'|} \tag{s2}$$

where Z_A is the charge of nucleus A located at R_A.

The v-basins are obtained like ρ-basins: the regions of v-basins are divided by surfaces of zero flux in the gradient vectors of electrostatic potential. The v-basin of each nucleus demonstrates the region where the electron density is attracted by that nucleus. Thus, the superposition of gradient fields of the electrostatic potential and the electron density clearly illustrates the electrostatic nature of the interactions in the crystal.

The deformation density function is used to illustrate the redistribution of electrons taking place in a system when the latter is formed from free atoms [17]:

$$\delta\rho(r)=\rho(r)-\rho(r)_{pro} \tag{s3}$$

where $\rho(r)$ is the electron density of the crystal (with relaxed geometry) and $\rho(r)_{pro}$ is the sum of the electron densities of the spherical non-interacting atoms placed at the same positions as the atoms of the system.

The Cambridge Structural Database analysis

Version 5.39 (August 2018) of Cambridge Structural Database [18] was used to analyze the geometric features of the studied intermolecular interactions. The lengths of C-H bonds were normalized to an average neutron-diffraction value (1.089 Å) by moving the hydrogens along their valence-bonds. The cone correction was used to analyze the preferred C–H···F angle in C–H···F–C interactions [19]. This correction is usually used to eliminate the geometrical bias from the statistical data on different intermolecular interactions, such as halogen bonds [19] and C–H···F/O contacts [20, 21].

Table S1. Experimental and theoretical (PBE/6-31(F+)G**) values of the H…F and C…F distances in Synthons A and D (Fig. 1).

Synthon A			
Distance	Crystalline ***m*-$C_6H_2F_4$** [22]		Cluster model
	Experiment	Periodic DFT	
H…F	2.531[a)]	2.562	2.401
C…F	3.565	3.428	3.420
Synthon D			
Distance	cocrystal of C_6F_6 and anthracene (ZZZGMW01) [2]		Cluster model
	Experiment	Periodic DFT	
H…F	2.520[a)]	2.425	2.496
C…F	3.508	3.421	3.494

[a)] the experimental value is given of C–H bonds were normalized to 1.08 Å [22]

Table S2. Root-mean-square errors of the experimental values of intermolecular C-F···F-C distances from the corresponding theoretical values calculated in different approximations. The root-mean-square error values of contacts shorter than 2.94 Å are parenthesized if exist. The CSD refcodes of the considered crystals are given in parentheses. The minimal error values are given in bold.

Approximation	**CF_4** (TFMETH03)	**C_6F_6** (HFBENZ02)	**C_6F_5COOH** (PFBZAC01)	**C_5NHF_4** (DATLIV01)	**C_5NF_5** (RITNOY02)
B3LYP/6-31G**	0.1745	0.0854 (0.0464)	**0.0298** (0.0299)	0.0257 (0.0162)	- [a)]
B3LYP-D3/6-31G**	0.1900	0.0861 (0.0508)	0.0448 (0.0269)	0.0332 (0.0183)	0.1986 (0.1217)
B3LYP/6-31(F+)G**	0.0702	**0.030** (0.0222)	-	**0.0178** (0.0154)	0.0660 (0.0493)
B3LYP/pob-TZVP	0.0394	0.1227 (0.0609)	0.0615 (0.0279)	0.0525 (0.0115)	0.0852 (0.0903)
PBE/6-31G**	0.0910	0.0866 (0.0584)	0.0513 (0.0319)	0.0303 (0.0358)	0.2234 (0.1272)
PBE-D3/6-31G**	0.1173	0.0861 (0.0598)	0.0586 (0.0292)	0.0357 (0.0374)	0.1807 (0.1040)
PBE/6-31(F+)G**	0.0668	0.0471 (0.0377)	0.0416 (0.0242)	0.0309 (0.0355)	0.0560 (0.0541)
PBE-D3/6-31(F+)G**	**0.0647**	0.0428 (0.0368)	0.0507 (0.0278)	0.0346 (0.0350)	**0.0345** (0.0336)
PBE/pob-TZVP	0.0910	0.0866 (0.0584)	0.0822 (0.0375)	0.0546 (0.0318)	0.0728 (0.0733)

[a)] Empty field means that convergence of SCF procedure was not achieved, or the conducted state was achieved during optimization.

Table S3. Experimental and theoretical values of the electron density, ρ_b, and the Laplacian of the electron density, $\nabla^2\rho_b$, at the (3,-1) critical point of the C-F···F-C interactions.

Refcode	XRD			PBE-D3/6-31(F+)G**			
	R(F···F), Å	ρ_b, a.u. [a)]	$\nabla^2\rho_b$, a.u.	R(F···F), Å	ρ_b, a.u.	$\nabla^2\rho_b$, a.u.	E_{int}, [c)] kJ/mol
C_5NHF_4 [10]	2.921	0.0044(15)	0.025	2.876	0.0056	0.0296	2.2
without H-bond(s)	3.048	0.0030(15)	0.021	3.092	0.0044	0.0248	1.7
	3.131	0.0030(15)	0.017	3.085	0.0034	0.0202	1.4
GEYLOL01 [11]	2.862	0.0059(15)	0.033	2.846	0.0062	0.0324	2.4
without H-bond(s)	3.083	0.0044(15)	0.021	3.059	0.0036	0.0214	1.4
	3.198	0.0030(15)	0.017	3.187	0.0031	0.0186	1.2
BENAFP02 [12] with H-bond(s)	2.819	0.0059(15)	0.034	2.818	0.0073	0.0349	2.7
C_6F_5COOH [9]	2.637	0.0086(2)	0.051	2.644	0.0090	0.0450	3.5
with H-bond(s)	2.628	0.0099(2)	0.059	2.601	0.0106	0.0506	4.0
KETVUC01 [13]	2.664	0.0089(15)	0.054	2.672	0.0100	0.0487	3.8
with H-bond(s)	2.825	0.0059(15)	0.037	2.737[b)]	0.0086	0.0407	3.2
	2.967	0.0044(15)	0.025	2.889	0.0059	0.0309	2.2

[a)] Accuracy of the measurements is specified in brackets;

[b)] Please note that the biggest difference between experimental and theoretical ρ_b values corresponds to the greatest difference between experimental and theoretical C-F···F-C distance. If the experimental and theoretical F···F distances are close, then ρ_b values are close too;

[c)] E_{int} evaluated using Eq. (3) with the coefficient equals to 0.129 is given in the last column.

Table S4. Theoretical values of the lattice energy (kJ/mol) of crystalline **CF_4**, **C_6F_6** and **C_6F_5COOH** obtained using Eq. (1), with different levels of periodic DFT computations.[a)]

Approximation	**CF_4**	**C_6F_6**	**C_6F_5COOH**
B3LYP/6-31G* [b)]	-7.3	-14.4	18.9
B3LYP-D3/6-31G*	20.9	101.1	182.9
B3LYP-D3-gCP/6-31G* [c)]	-610.8	-506.4	-301.2
B3LYP/pob-TZVP	-9.0	-8.9	25.9
PBE/6-31(F+)G** [b)]	-1.7	1.5	41.8
PBE-D3/6-31(F+)G**	17.1	69.8	143.6
Experimental ΔH_{sub}	14.0-17.0	46.0-49.8	92.0

[a)] BSSE correction using the Boys-Bernandi counterpoise scheme [23] was taken into account;
[b)] Please note that 6-31G* and 6-31G** basis sets are equivalent for **CF_4** and **C_6F_6** crystals, since these crystals do not contain hydrogen atoms;
[c)] BSSE correction was not considered in calculations using the gCP correction [24].

Table S5. Comparison of the E_{latt} values of crystals of perfluorinated molecules evaluated using Eq. (2) with the ΔH_{sub} experimental values. The units are kJ/mol.

Crystal	PIXEL	Eq. (3) [a)]		ΔH_{sub} [25]
	MP2/6-31G**[b)]	B3LYP/6-31G*	B3LYP-D3/6-31G*	
CF_4	12.3	42.6 (69.5)	52.7 (65.5)	14.0-17.0
C_6F_6	-[c)]	71.7 (77.3)	67.3 (72.7)	46.0-49.8
C_6F_5COOH	77.5	128.3 (130.5)	120.7 (123.2)	92.0

[a)] E_{latt} was evaluated for intermolecular interactions with $\rho_b > 0.003$ a.u.; the corresponding values of the lattice energy computed with account of all interactions is given in parenthesis;
[b)] Default level of theory used in Gaussian SCF calculations to build the electron density grid of an isolated molecule;
[c)] PIXEL approach is inapplicable to crystals with Z' = 1.5.

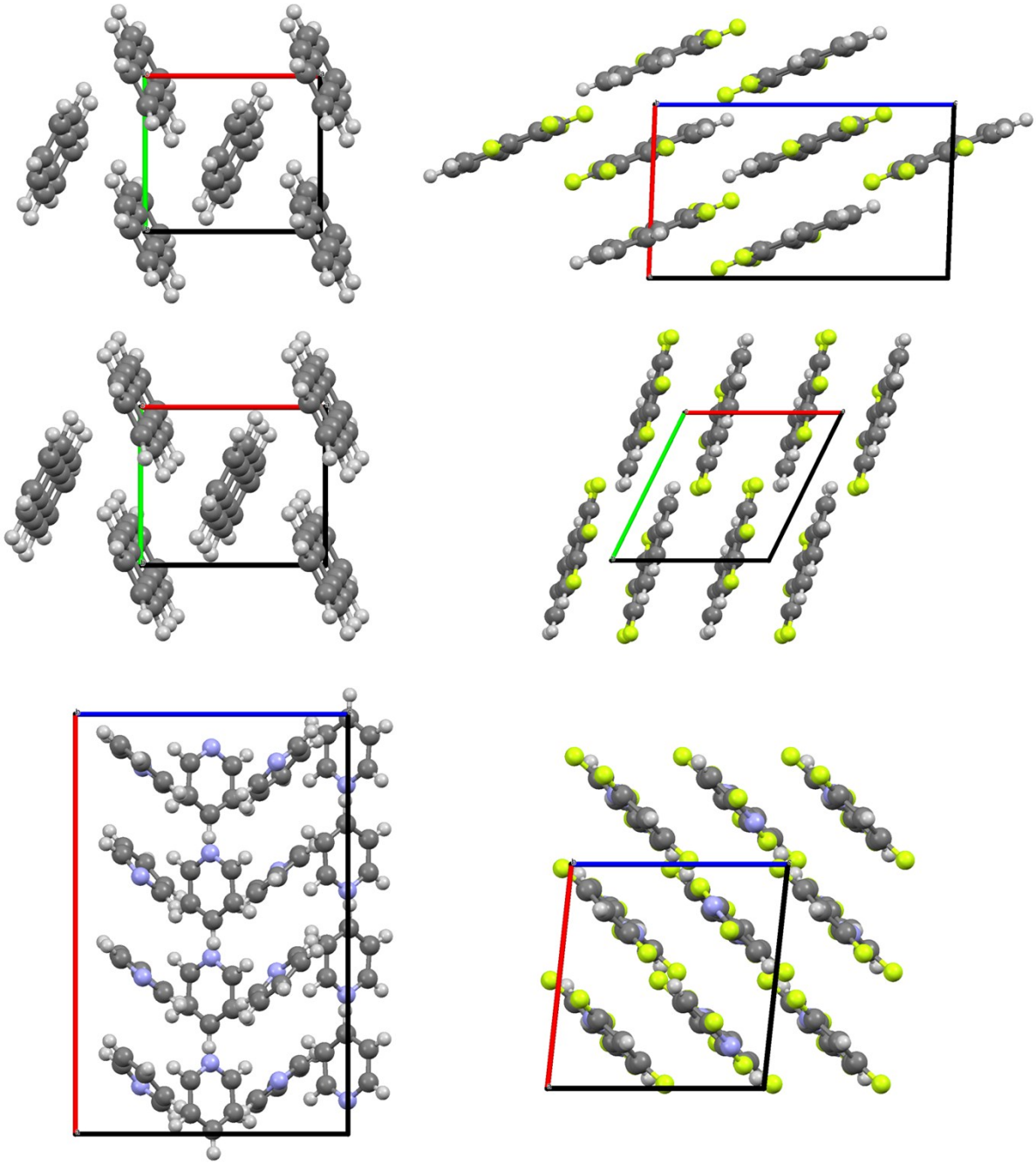

Figure S1. Transformation of crystal packing with partial fluorination of some organic compounds. The CSD refcodes of the considered crystals are given in parentheses. Upper panel: naphthalene (NAPHTA33 [26]) and 1,2,3,4-tetrafluoronaphthalene (CAXNUL06 [27]). Middle panel: anthracene (ANTCEN16 [28]) and 1,2,3,4-tetrafluoroanthracene (MIKGOD01 [27]). Lower panel: pyridine (PYRDNA06 [29]) and 2,4,6-trifluoropyridine (MAGWUO [30]).

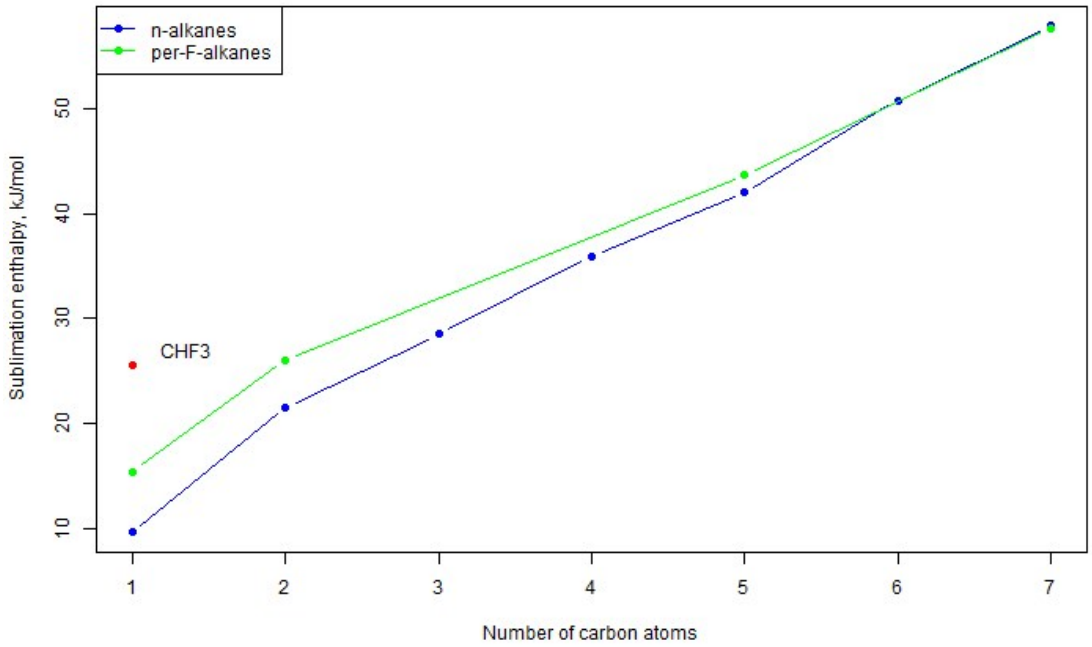

Figure S2. Sublimation enthalpies of alkanes (blue), perfluoroalkanes (green) and the only partially fluorinated alkane CHF_3 [25].

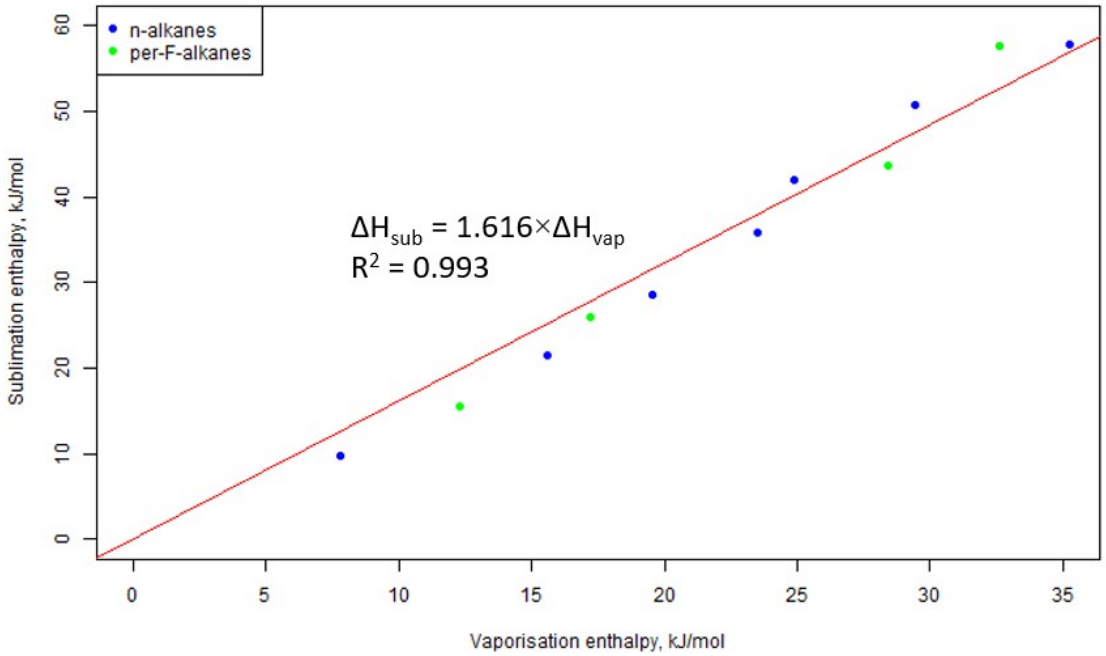

Figure S3. Correlation between sublimation and vaporization enthalpies of alkanes (blue) and perfluoroalkanes (green) [25].

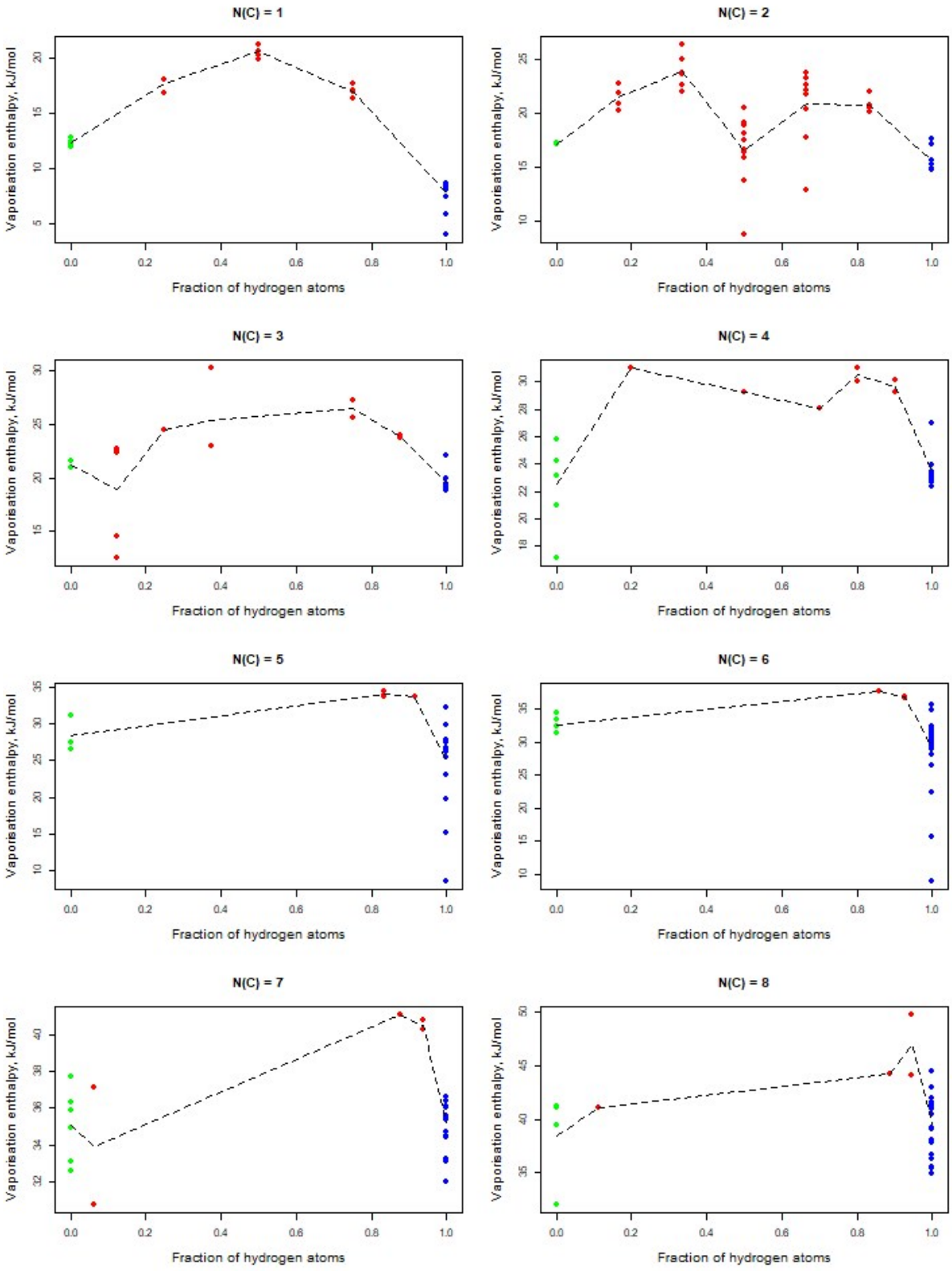

Figure S4. Dependence of vaporization enthalpy of fluoroalkanes on a fraction of hydrogen atoms, $n_H/(n_F + n_H)$ [25]. Green, red and blue points correspond to perfluoroalkanes, partially fluorinated alkanes and alkanes, respectively.

Table S6. Metric and topological characteristics of C–H···F, C-H···O interactions in **KEGWEZ**, **DFNAPQ** and **YICBES** evaluated using periodic DFT calculations. ρ_b is electron density and $\nabla^2\rho(r)$ is the Laplacian of the electron density at the (3,-1) critical point of the H···F/H···O interactions. E_{int} is the energy of the corresponding interaction, evaluated using Eq. (3).

Contact[a)]	H···F/H···O distance, Å [b)]	$\rho(r)$, a.u.	$\nabla^2\rho(r)$, a.u.	E_{int}, kJ/mol
KEGWEZ				
C4-H1···O2 [c)]	2.125 (2.249)	0.0178	0.052	14.6 [c)]
C7-H2···O2	2.496 (2.484)	0.0079	0.028	6.8
C9-H4···O2	2.846 (2.940)	0.0043	0.016	3.4
C11-H6···F2	2.453 (2.472)	0.0068	0.029	7.0
C8-H3···F1	2.538 (2.582)	0.0066	0.029	6.7
C9-H4···F2	2.693 (2.664)	0.0047	0.021	4.6
C10-H5···F1	2.708 (2.733)	0.0054	0.025	5.4
DFNAPQ				
C8-H18···O14	2.449 (2.545)	0.0102	0.035	8.7
C6-H16···O11	2.464 (2.618)	0.0084	0.033	7.9
C7-H17···O14	2.681 (2.724)	0.0056	0.024	5.3
C15-H15···O11	2.746 (2.770)	0.0059	0.023	5.1
C6-H16···F13	2.459 (2.485)	0.0069	0.030	7.1
C7-H17···F12	2.466 (2.502)	0.0069	0.029	7.0
C15-H15···F12	2.559 (2.678)	0.0058	0.025	5.7
YICBES				
C5-H10···O1	2.233 (2.473)	0.0148	0.044	12.1 [c)]
C3-H2···O1	2.345 (2.500)	0.0116	0.037	9.6
C11-H5···F2	2.475 (2.454)	0.0073	0.031	7.3
C14-H8···F1	2.565 (2.552)	0.0060	0.025	5.8
C9-H4···F2	2.621 (2.800)	0.0053	0.023	5.1
C13-H7···F1	2.681 (2.829)	0.0051	0.022	5.0

[a)] see Figs. 7 and S5 for atom numeration;
[b)] the experimental values are given in parentheses (C-H bonds were normalized to 1.089 Å);
[c)] a relatively large energies of the C4-H1···O2 contacts is caused by strong underestimation of the H1···O2/H10···O1 distances by periodic DFT computations.

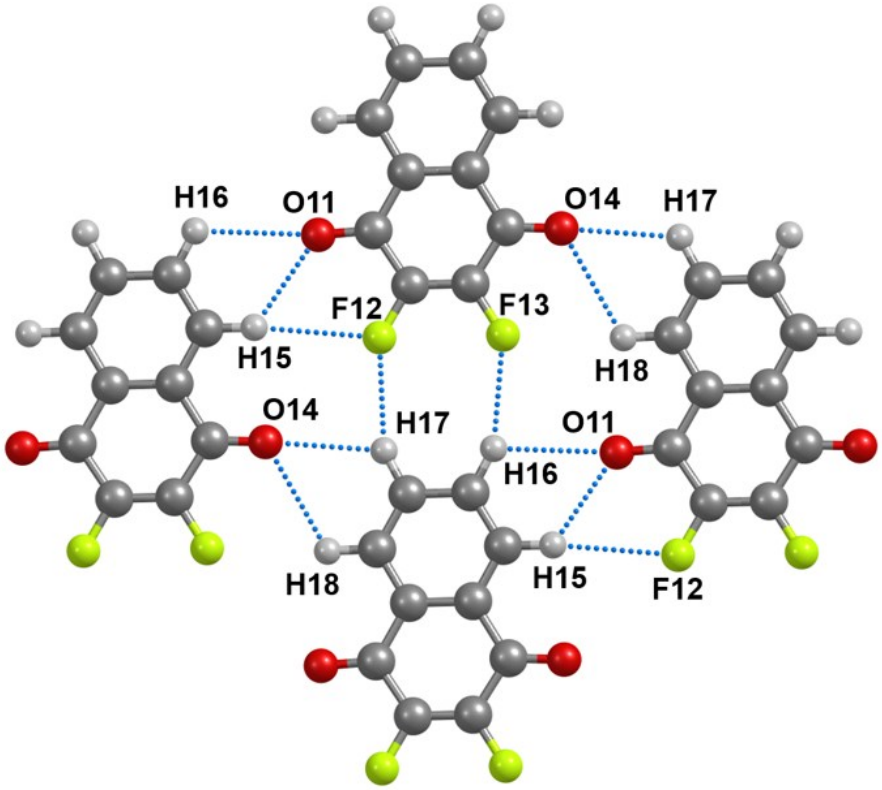

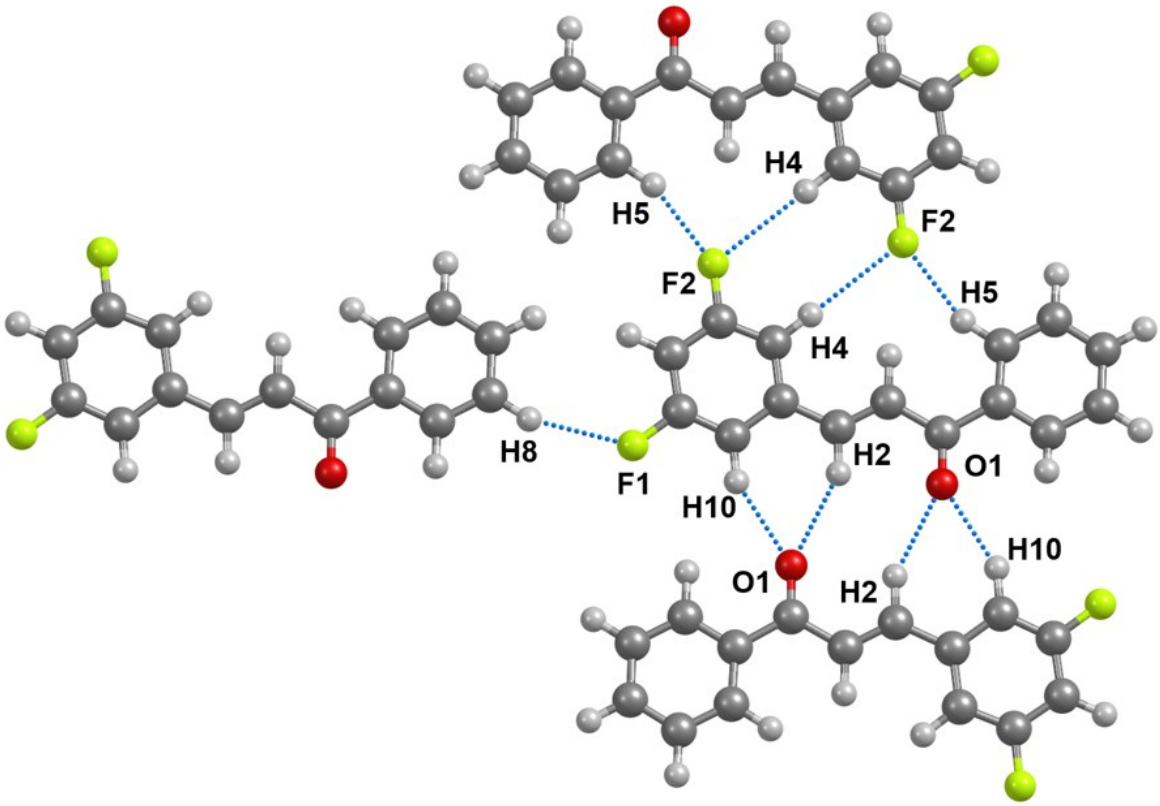

Figure S5. The fragments of crystalline **DFNAPQ** (upper panel) and **YICBES** (lower panel). Atoms forming the C–H···F–C, C–F···F–C, C–H···O interactions are labeled.

Table S7. Metric and topological characteristics of the selected intermolecular interactions in **OVIHAD, OVIHEH** and **OVIHIL** evaluated using periodic DFT calculations. ρ_b is electron density and $\nabla^2\rho(r)$ is the Laplacian of the electron density at the (3,-1) critical point of the H···S/H···F/H···O interactions. E_{int} is the energy of the corresponding interaction, evaluated using Eq. (3).

Contact[a)]	H···S[b)]/H···F/H···O distance, Å [c)]	ρ(r), a.u.	$\nabla^2\rho$(r), a.u.	E_{int}, [d)] kJ/mol
OVIHAD				
N2–H···S	2.321 (2.594)	0.023	0.046	14.2
C–H13···O	2.440 (2.592)	0.009	0.031	7.6
C–H4···F2	2.784 (2.859)	0.004	0.021	4.4
C–H10···F1	2.652 (2.820)	0.005	0.023	5.2
C–H3···F2	2.447 (2.598)	0.007	0.033	7.6
C–F2···F1	3.163 (3.125)	0.003	0.019	1.2
OVIHEH				
N2–H···S	2.601 (2.908)	0.013	0.032	8.2
C–H3···O	2.571 (2.693)	0.008	0.029	6.9
C–H2···O	2.576 (2.666)	0.007	0.028	6.6
C–H11···F1	2.365 (2.460)	0.010	0.041	9.9
C–H4···F1	2.651 (2.853)	0.005	0.021	4.7
C–H11'···F1	2.903 (2.978)	0.003	0.015	3.0
OVIHIL				
N2–H···S	2.431 (2.781)	0.019	0.039	11.4
C–H3···O	2.248 (2.513)	0.015	0.043	11.9
C–H5···F2	2.494 (2.732)	0.007	0.031	7.4
C–H13···F1	2.268 (2.458)	0.012	0.042	11.3
C–H2···F1	2.427 (2.603)	0.007	0.032	7.6
C–H11···F2	2.407 (2.613)	0.009	0.035	8.6
C–F2···F2	3.131 (3.003)	0.004	0.023	1.5

[a)] see Fig. S6 for atomic numeration;
[b)] C–H···S interactions were also localized during topological analysis of electron density: 4, 5 and 3 unique CP(H···S) for OVIHAD, OVIHEH and OVIHIL, correspondingly. E_{int} of C–H···S interactions is comparable to E_{int} of C–H···O interactions;
[c)] the experimental values are given in parentheses;
[d)] in the case of the F···F contacts the coefficient value in Eq. (3) equals to 0.129 (Subsection 3.2).

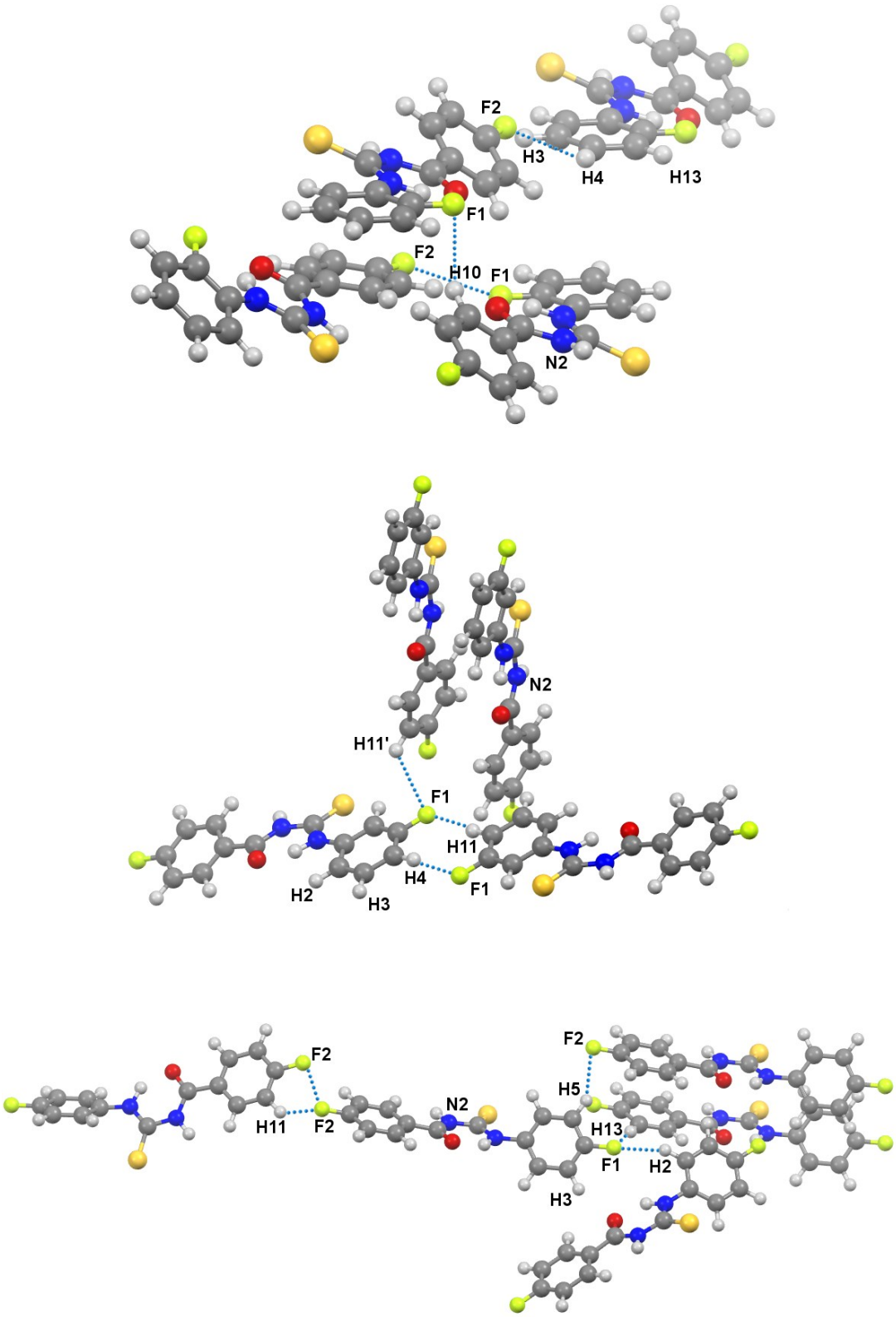

Figure S6. Fragments of crystalline **OVIHAD** (upper panel), **OVIHEH** (middle panel) and **OVIHIL** (lower panel). The C–H···F–C and C–F···F–C interactions are denoted by dotted lines. Red atoms = O, blue atoms= N, yellow atoms = F, grey atoms = C, light gray atoms = H and orange atoms = S.

C–H···F–C and C–F···F–C interactions in presence of conventional H-bonds

The metric parameters and energies of C–H···F–C/ C–F···F–C interactions in crystals with conventional H-bonds (**C_6F_5COOH**, **TISQER** and **R_fCOOH**) are given in Tables S8 and S9. The appearance of relatively strong interactions has practically no effect on the H···F distances, compared with crystals containing only C, H and F atoms [31]. The C–H···F–C energies are maximum for 2.50 - 2.60 Å and range from ~ 5 to ~ 7 kJ/mol (Subsection 3.3 and Table 5 in Ref. [32]). The C–F···F–C distances become shorter in H-bonded crystals than those in crystals containing only C, H and F atoms. As a result, the average energy of the F···F interactions increases from ~ 2 to ~ 4 kJ/mol (Table S3). Conventional H-bonds are much stronger than C–H···F–C interactions (Tables S8 and S9) and have the major impact on the lattice energy of organic crystals [33]. As a result, C–H···F–C interactions lose their structure-directing role in the presence of conventional O–H···O bonds [34].

Table S8. Metric and topological characteristics of the C–H···F–C, C–F···F–C contacts and the conventional H-bonds in crystalline **TISQER** and **C_6F_5COOH** evaluated using periodic DFT calculations at the PBE-D3/6-31(F+)G** level. ρ_b is electron density, $\nabla^2\rho(r)$ is the Laplacian of the electron density, $\lambda_1, \lambda_2, \lambda_3$ are electron density curvatures at the (3,-1) critical point of the H···F/F···F contacts and H-bonds. E_{int} is the energy of the corresponding contact, evaluated using Eq. (3).

Contact[a)]	H···F/F···F/H···O distance, Å [b)]	ρ(r), a.u.	$\nabla^2\rho$(r), a.u.	λ_1, a.u.	λ_2, a.u.	$\lvert\lambda_1/\lambda_3\rvert$	E_{int}, [c)] kJ/mol
TISQER							
O5-H9···O1	1.667	0.050	0.111	-0.099	-0.094	0.324	42.8
O1-H8···O5	1.730	0.041	0.113	-0.075	-0.073	0.288	37.4
C3-H3···F1-C4	2.186 (2.358)	0.015	0.054	-0.019	-0.018	0.209	13.1 [d)]
C2-H2···F1-C4	2.502 (2.586)	0.007	0.034	-0.008	-0.005	0.162	7.2
C_6F_5COOH							
O2-H1···O1	1.559	0.0694	0.151	-0.145	-0.144	0.327	55.3
C5-F4···F4-C5	2.601 (2.627)	0.0106	0.051	-0.010	-0.010	0.141	4.0
C4-F3···F3-C4	2.645 (2.637)	0.0090	0.045	-0.009	-0.008	0.145	3.5
C3-F2···F5-C6	2.713 (2.760)	0.0081	0.040	-0.008	-0.008	0.143	3.1
C3-F2···F3-C4	2.860 (2.855)	0.0074	0.036	-0.008	-0.007	0.157	2.7
C2-F1···F4-C5	2.875 (2.828)	0.0074	0.037	-0.007	-0.006	0.140	2.8

[a)] see Fig. S7 for atom numeration;

[b)] the experimental values are given in parentheses (C-H bonds were normalized to 1.09 Å);

[c)] in the case of the F···F contacts the value of the coefficient in Eq. (3) equals to 0.129 (Subsection 3.2);

[d)] a relatively large energy of the C3-H3···F1-C4 contact is caused by strong overestimation of the H3···F1 by periodic DFT computations.

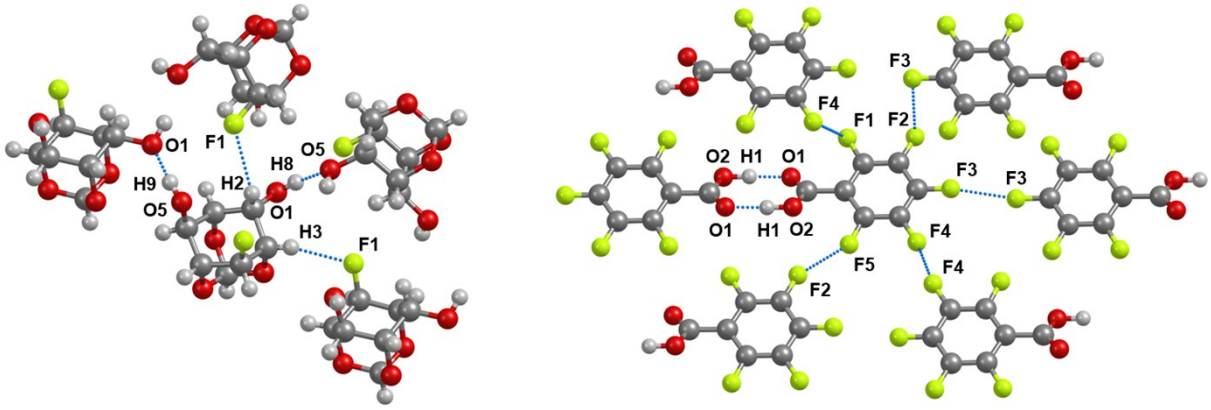

Figure S7. Fragment of **TISQER** (left panel) and **C_6F_5COOH** (right panel). Atoms forming the C–H···F–C, C–F···F–C, C–H···O and O–H···O interactions are labeled.

Table S9. Metric and topological characteristics of the C–H···F, C–F···F, C-H···O interactions and the conventional H-bonds in **R_fCOOH** evaluated using periodic DFT calculations. ρ_b is electron density, $\nabla^2\rho(r)$ is the Laplacian of the electron density, $\lambda_1, \lambda_2, \lambda_3$ are electron density curvatures at the (3,-1) critical point of the H···F/F···F interactions and H-bonds. E_{int} is the energy of the corresponding interaction, evaluated using Eq. (3).

Contact[a)]	H···F/F···F/H···O distance, Å [b]	ρ(r), a.u.	$\nabla^2\rho$(r), a.u.	λ_1, a.u.	λ_2, a.u.	$\lvert\lambda_1/\lambda_3\rvert$	E_{int}, [c)] kJ/mol
R_fCOOH							
O2-H1···O1	1.537	0.0747	0.151	-0.160	-0.158	0.340	59.4
C2-H2···O1	2.452 (2.526)	0.0105	0.032	-0.011	-0.010	0.204	8.5
C4-H6···O1	2.645 (2.788)	0.0069	0.024	-0.006	-0.005	0.167	5.9
C3-H4···O2	2.707 (2.705)	0.0055	0.020	-0.005	-0.005	0.167	4.8
C9-H17···F1	2.575 (2.568)	0.0059	0.025	-0.006	-0.006	0.162	5.8
C8-H15···F1	2.614 (2.611)	0.0061	0.025	-0.006	-0.005	0.167	5.7
C13-F3···F4	2.865 (2.864)	0.0067	0.034	-0.007	-0.007	0.149	2.5
C12-F2···F3	2.914 (2.925)	0.0059	0.030	-0.006	-0.005	0.146	2.2

[a)] see Figs. S8 for atom numeration;
[b)] the experimental values are given in parentheses (C-H bonds were normalized to 1.09 Å);
[c)] in the case of the F···F contacts the value of the coefficient in Eq. (1) equals to 0.129 (Subsection 3.2);
[d)] a relatively large energy of the C4-H1···O2 contact is caused by strong overestimation of the H1···O2 by periodic DFT computations.

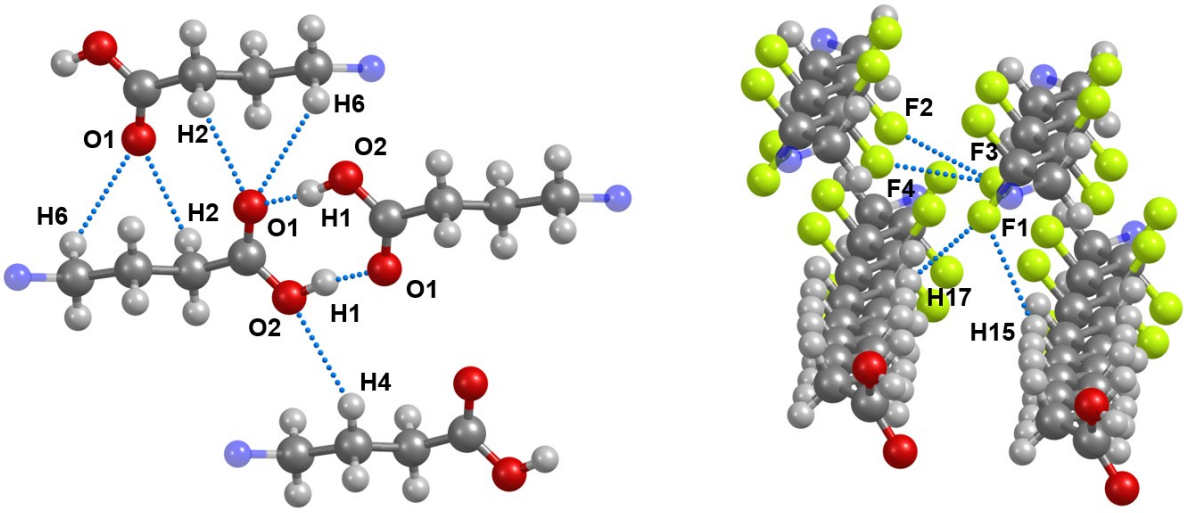

Figure S8. Fragment of **R_fCOOH**. Hydrogen and fluorine atoms forming the C–H···F–C and C–F···F–C contacts are labeled. Only part of each molecule is shown, with blue transparent spheres denoting the truncated fragments.

References

1. P. Giannozzi, S. Baroni, N. Bonini, M. Calandra, R. Car, C. Cavazzoni, D. Ceresoli, G. L. Chiarotti, M. Cococcioni, I. Dabo, A. Dal Corso, S. Fabris, G. Fratesi, S. de Gironcoli, R. Gebauer, U. Gerstmann, C. Gougoussis, A. Kokalj, M. Lazzeri, L. Martin-Samos, N. Marzari, F. Mauri, R. Mazzarello, S. Paolini, A. Pasquarello, L. Paulatto, C. Sbraccia, S. Scandolo, G. Sclauzero, A. P. Seitsonen, A. Smogunov, P. Umari, and R. M. Wentzcovitch, QUANTUM ESPRESSO: a modular and open-source software project for quantum simulations of materials, *J. Phys.: Condens. Matter* **2009**, *21*, 395502.

2. P. Giannozzi, O. Andreussi, T. Brumme, O. Bunau, M. Buongiorno Nardelli, M. Calandra, R. Car, C. Cavazzoni, D. Ceresoli, M. Cococcioni, N. Colonna, I. Carnimeo, A. Dal Corso, S. de Gironcoli, P. Delugas, R. A. DiStasio Jr., A. Ferretti, A. Floris, G. Fratesi, G. Fugallo, R. Gebauer, U. Gerstmann, F. Giustino, T. Gorni, J. Jia, M. Kawamura, H.-Y. Ko, A. Kokalj, E. Küçükbenli, M. Lazzeri, M. Marsili, N. Marzari, F. Mauri, N. L. Nguyen, H.-V. Nguyen, A. Otero-de-la-Roza, L. Paulatto, S. Poncé, D. Rocca, R. Sabatini, B. Santra, M. Schlipf, A. P. Seitsonen, A. Smogunov, I. Timrov, T. Thonhauser, P. Umari, N. Vast, X. Wu and S. Baroni, Advanced capabilities for materials modelling with Quantum ESPRESSO, *J. Phys.: Condens. Matter* **2017**, *29*, 465901.

3. N. Troullier and J. L. Martins, Efficient pseudopotentials for plane-wave calculations, Phys. Rev. B **1991**, *43*, 1993–2006.

4. C. Hartwigsen, S. Goedecker and J. Hutter, Relativistic separable dual-space Gaussian pseudopotentials from H to Rn, *Phys. Rev. B* **1998**, *58*, 3641.

5. A. M. Rappe, K. M. Rabe, E. Kaxiras and J. D. Joannopoulos, Optimized pseudopotentials, *Phys. Rev. B* **1990**, *41*, 1227.

6. A. Dal Corso, Pseudopotentials periodic table: From H to Pu, *Comp. Mater. Sci.* **2014**, *95*, 337–350.

7. P. E. Blöchl, Projector augmented-wave method, *Phys. Rev. B* **1994**, *50*, 17953.

8. S. Tosoni, C. Tuma, J. Sauer, B. Civalleri and P. Ugliengo, A comparison between plane wave and Gaussian-type orbital basis sets for hydrogen bonded systems: formic acid as a test case, *J. Chem. Phys.* **2007**, *127*, 154102.

9. A. Bach, D. Lentz and P. Luger. Charge Density and Topological Analysis of Pentafluorobenzoic Acid, *J. Phys. Chem. A* **2001**, *105*, 7405–7412.

10. H.-G. Stammler, Y. V. Vishnevskiy, C. Sicking and N. W. Mitzel, Charge density studies on 2,3,5,6-tetrafluoro- and pentafluoropyridine, *CrystEngComm*, **2013**, *15*, 3536–3546.

11. D. E. Hibbs, J. Overgaard, J. A. Platts, M. P. Waller and M. B. Hursthouse, Experimental and Theoretical Charge Density Studies of Tetrafluorophthalonitrile and Tetrafluoroisophthalonitrile, *J. Phys. Chem. B* **2004**, *108*, 3663–3672.

12. V. R. Hathwar and T. N. Guru Row, Charge Density Analysis of Heterohalogen (Cl···F) and Homohalogen (F···F) Intermolecular Interactions in Molecular Crystals: Importance of the Extent of Polarizability, *Cryst. Growth Des.* **2011**, *11*, 1338–1346.

13. R.B.K. Siram, D. P. Karothu, T. N. Guru Row, S. Patil, Unique Type II Halogen···Halogen Interactions in Pentafluorophenyl-Appended 2,2′-Bithiazoles, *Cryst. Growth Des.* **2013**, *13*, 1045–1049.

14. A. Zapata, B. Bernet and A. Vasella, Glycosylidene Carbenes. Part 23. Regioselective glycosidation of deoxy- and fluorodeoxy-myo-inositol derivatives, *Helv. Chim. Acta* **1996**, *79*, 1169–1191.

15. P. Beier, D. O'Hagan, C. Pearson, M. C. Petty and A. M. Z. Slawin, The structure and properties of hybrid fluorous-hydrocarbon fatty acids, *J. Fluorine Chem.* **2005**, *126*, 671–680.

16. A. Saeed, M. F. Erben, U. Shaheen, U. Flörke, Synthesis, structural and vibrational properties of 1-(4-Fluorobenzoyl)-3-(isomeric fluorophenyl)thioureas, *J. Mol. Struct.* **2011**, *1000*, 49–57.

17. R. F. W. Bader, Atoms in molecules. Quantum Theory, Oxford: Clarengon press, 1994, p. 432.

18. C. R. Groom, I. J. Bruno, M. P. Lightfoot and S. C. Ward, The Cambridge Structural Database, *Acta Cryst.* **2016**, *B72*, 171–179.

19. B. K. Saha, S. A. Rather, A. Saha, Interhalogen Interactions in the Light of Geometrical Correction, *Cryst. Growth Des*. **2016**, *16*, 3059–3062.

20. B. K. Saha, A. Saha, D. Sharada and S. A. Rather, F or O, Which One Is the Better Hydrogen Bond (Is It?) Acceptor in C–H···X–C (X– = F–, O═) Interactions? *Cryst. Growth Des.* **2018**, *18*, 1–6.

21. A. Saha, S. A. Rather, D. Sharada and B. K. Saha, Sodium Induces Octacalcium Phosphate Formation and Enhances Its Layer Structure by Affecting the Hydrous Layer Phosphate. *Cryst. Growth Des*. **2018**, *18*, 6084–6090.

22. T. S. Thakur, M. T. Kirchner, D. Bläser, R. Boese and G. R. Desiraju, G. R. C–H···F–C hydrogen bonding in 1,2,3,5-tetrafluorobenzene and other fluoroaromatic compounds and the crystal structure of alloxan revisited, *CrystEngComm* **2010**, *12*, 2079−2085.

23. S.F. Boys, F.D. Bernardi, The calculation of small molecular interactions by the differences of separate total energies. Some procedures with reduced errors. *J. Mol. Phys.* **1970**, *19*, 553-566.

24. J. G. Brandenburg, M. Alessio, B. Civalleri, M. F. Peintinger, T. Bredow and S. Grimme, Geometrical Correction for the Inter- and Intramolecular Basis Set Superposition Error in Periodic Density Functional Theory Calculations, *J. Phys. Chem. A* **2013**, *117*, 9282–9292.

25. J. S. Chickos and W. E. Acree, Phase Transition Enthalpy Measurements of Organic and Organometallic Compounds. Sublimation, Vaporization and Fusion Enthalpies From 1880 to 2010, *J. Phys. Chem. Ref. Data* **2010**, *39*, 043101.

26. S. C. Capelli, A. Albinati, S. A. Mason and B. T. M. Willis, Molecular Motion in Crystalline Naphthalene: Analysis of Multi-Temperature X-Ray and Neutron Diffraction Data, *J. Phys. Chem. A* **2006**, *110*, 11695–11703.

27. F. Cozzi, S. Bacchi, G. Filippini, T. Pilati and A. Gavezzotti, Synthesis, X-ray Diffraction and Computational Study of the Crystal Packing of Polycyclic Hydrocarbons Featuring Aromatic and Perfluoroaromatic Rings Condensed in the Same Molecule: 1,2,3,4-Tetrafluoronaphthalene, -anthracene and -phenanthrene, *Chem. Eur. J.* **2007**, *13*, 7177–7184.

28. S. L. Chaplot, N. Lehner and G. S. Pawley, The structure of anthracene-d_{10} at 16 K using neutron diffraction, *Acta Cryst.* **1982**, *B38*, 483–487.

29. M. Podsiadlo, K. Jakobek and A. Katrusiak, Density, freezing and molecular aggregation in pyridazine, pyridine and benzene, *CrystEngComm* **2010**, *12*, 2561–2567.

30. V. Vasylyeva and K. Merz, Aggregation of fluorine-substituted pyridines, *J. Fluorine Chem.* **2010**, *131*, 446–449.

31. P. Panini and D. Chopra, Experimental and Theoretical Characterization of Short H‑Bonds with Organic Fluorine in Molecular Crystals, *Crystal Growth & Design* **2014**, 14, 3155−3168.

32. G. Kaur and A. R. Choudhury, A comprehensive understanding of the synthons involving C–H···F–C hydrogen bond(s) from structural and computational analyses, *CrystEngComm* **2015**, *17*, 2949–2963.

33. A. N. Manin, A. P. Voronin, N. G. Manin, M. V. Vener, A. V. Shishkina, A. S. Lermontov, G. L. Perlovich, Salicylamide Cocrystals: Screening, Crystal Structure, Sublimation, Thermodynamics, Dissolution, and Solid-State DFT Calculations, *J. Phys. Chem. B* **2014**, *118*, 6803–6814.

34. I. D. Madura, K. Czerwinska and D. Sołdanska, Hydrogen-Bonded Dimeric Synthon of Fluoro-Substituted Phenylboronic Acids versus Supramolecular Organization in Crystals, *Cryst. Growth Des.* **2014**, *14*, 5912–5921.